

Technical Note

Preparation of fixed mouse brains for MRI

Lindsay S. Cahill^{*}, Christine L. Laliberté, Jacob Ellegood, Shoshana Spring, Jacqueline A. Gleave, Matthijs C. van Eede, Jason P. Lerch, R. Mark Henkelman

Mouse Imaging Centre, The Hospital for Sick Children, Toronto, Ontario, Canada

ARTICLE INFO

Article history:

Received 15 October 2011

Revised 23 December 2011

Accepted 18 January 2012

Available online 28 January 2012

Keywords:

Mouse brain

Tissue fixation

Perfusion

Paraformaldehyde

MRI

ABSTRACT

In fixed mouse brain magnetic resonance images, a high prevalence of fixation artifacts have been observed. Of more than 1700 images of fixed brains acquired at our laboratory, fixation artifacts were present in approximately 30%. In this study, two of these artifacts are described and their causes are identified. A hyperintense rim around the brain is observed when using perfusates reconstituted from powder and delivered at a high flow rate. It is proposed that these perfusion conditions cause blockage of the capillary beds and an increase in pressure that ruptures the vessels, resulting in a blister of liquid below the dura mater. Secondly, gray–white matter contrast inversion is observed when too short a fixation time or too low a concentration of fixative is used, resulting in inadequate fixation. The deleterious consequences of these artifacts for quantitative data analysis are discussed, and precautions for their prevention are provided.

© 2012 Elsevier Inc. All rights reserved.

Introduction

High resolution magnetic resonance imaging (MRI) of fixed mouse brains has become a powerful tool in biological research. Its applications include digital atlasing (Badea et al., 2007; Dorr et al., 2008; Ma et al., 2005), measurement of water diffusion (Chuang et al., 2011; Song et al., 2005; Zhang et al., 2003, 2010) and the study of genetic mutations (Ellegood et al., 2011; Ho et al., 2009; Kim et al., 2011; Mercer et al., 2009), disease models (Ellegood et al., 2010; Lau et al., 2008; Lerch et al., 2008a, 2008b; Sawiak et al., 2009; Wetzel et al., 2008), sexual dimorphism (Spring et al., 2007), brain development (Yu et al., 2011) and the effects of learning on brain plasticity (Lerch et al., 2011). The role of fixed mouse brain imaging will become increasingly important as the number of mouse mutants and mouse models of human diseases continue to grow.

Compared to live MR imaging, fixed imaging does not suffer from motion artifacts and allows for longer scan times and the use of non-physiological MR contrast agents, resulting in images with higher resolution and signal-to-noise ratio (SNR). For preparation of brain samples, transcardiac perfusion is preferred over immersion fixation because it

utilizes the vascular network to deliver fixative rapidly and evenly to the brain tissue.

Out of more than 1700 brains prepared by perfusion, we have seen MR artifacts in approximately 30%, predominantly in samples prepared by collaborating laboratories. Within this 30%, many of the MR images were unacceptable for quantitative data analysis. Fixed brain samples from 16 of 25 different collaborations showed anomalous signal intensities, with very few cases in which all the samples were affected. Communication with other mouse imaging laboratories confirmed that fixation artifacts are regularly present in fixed brain samples prepared at other facilities, indicating that this is a general problem. Each step of the sample preparation and the methods of storage (i.e. temperature) and transportation were explored to determine the causes of these artifacts. Here, two artifacts resulting from the transcardiac perfusion method of fixation are presented and the causes of these artifacts are identified. The results of this work emphasize the importance of perfusion flow rate, the form and concentration of perfusates and the timing of the protocol to eliminate fixation artifacts.

Material and methods

Animals

For exploring the causes of the artifacts, C57BL/6J mice from the Jackson Laboratory (Bar Harbor, ME) were used. All animal experiments were approved by the animal ethics committee of the Hospital for Sick Children (Toronto, ON).

^{*} Corresponding author at: Mouse Imaging Centre, The Hospital for Sick Children, 25 Orde Street, Toronto, Ontario, Canada M5T 3H7. Fax: +1 647 837 5832.

E-mail addresses: lcahill@phenogenomics.ca (L.S. Cahill), claliberte@phenogenomics.ca (C.L. Laliberté), jacob@phenogenomics.ca (J. Ellegood), sspring@phenogenomics.ca (S. Spring), jacqueline.gleave@phenogenomics.ca (J.A. Gleave), matthijs@phenogenomics.ca (M.C. van Eede), jason@phenogenomics.ca (J.P. Lerch), mhenkel@phenogenomics.ca (R.M. Henkelman).

Table 1

Summary of the number of MR images with rim/number of mice investigated for the different perfusion conditions used to determine the cause of the subdural hyperintense rim artifact.

PFA source	Powder	Liquid
Flow rate		
1 mL/min	4/8	0/4 ^a
7 mL/min	6/6	0/6

^a These perfusion conditions were only used four times in this specific study; however, this is the standard procedure used in our laboratory and therefore the total number of MR images that did not display any hyperintense rim is greater than 1000.

Perfusion protocols

Transcardiac perfusion was performed as described previously (Dazai et al., 2011; Spring et al., 2007; Tyszka et al., 2006). Briefly, animals were perfused through the left ventricle with 30 mL of phosphate-buffered saline (PBS) and 1 μ L/mL heparin (1000 USP units/mL). This was followed by infusion with 30 mL of 4% paraformaldehyde (PFA) in PBS for fixation. The effect of flow rate and the form of the PFA solution for fixation were both examined using four different perfusion conditions (Table 1). A peristaltic pump was connected to a pressure transducer to monitor the perfusion pressure. The effect of the concentration of PFA for fixation was also investigated. *Liquid PFA* (Electron Microscopy Sciences, #15710) is available in a 16% aqueous solution and is diluted with *liquid PBS* (Wisent, #311-010-CL) the same day as the

perfusion to produce a 4% PFA solution. For the remainder of this paper, we refer for brevity to this PFA source as “liquid”. *Powder PFA* (BioShop, #PAR070.1) was prepared the same day as the perfusion, dissolved in powder PBS under heat, stirred and filtered using coarse porosity filter paper. The *powder PBS* was made with sodium phosphate dibasic anhydrous (BioShop, #SPD307.1), sodium phosphate monobasic monohydrate (BioShop, #SPM306.1) and sodium chloride (BioShop, #SOD002.205) that was diluted in distilled water. This reconstituted PFA is subsequently referred to as “powder”. For all perfusion conditions, the temperature of the perfusates was maintained at room temperature and the pH of the PFA was 7.2–7.4.

Histology

Fixed brains were removed from the skull, paraffin-embedded and sectioned (4 μ m) on the sagittal plane. Tissue sections were stained with hematoxylin and eosin (H&E).

Magnetic resonance imaging

A multi-channel 7.0 T, 40 cm diameter bore magnet (Varian Inc. Palo Alto, CA) was used to acquire anatomical images. A custom-built 16-coil solenoid array was used to image 16 samples concurrently (Dazai et al., 2011). Parameters used in the scans were optimized for gray–white matter contrast: a T2-weighted 3D fast spin-echo sequence, with TR=2000 ms, echo train length=6, TE_{eff}=42 ms, field-of-view (FOV)=25×28×14 mm and matrix size=450×504×250, giving an image with 56 μ m

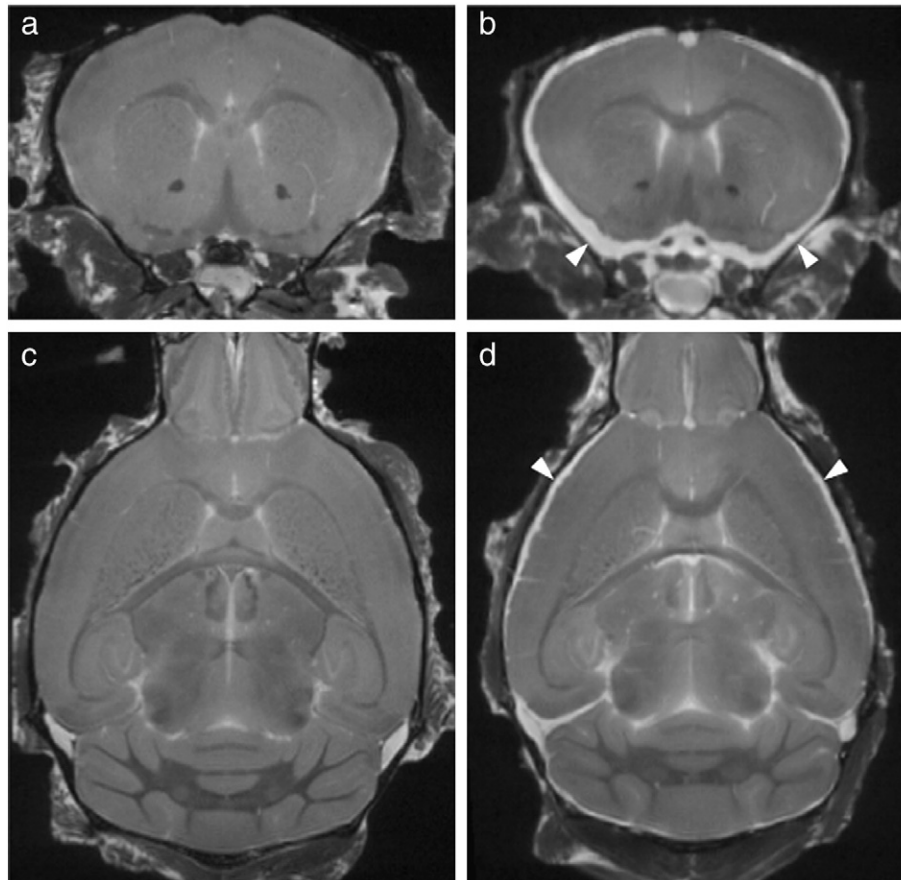


Fig. 1. Coronal (a) and axial (c) slices from a T2w MR image of a mouse perfused with liquid PFA and high flow rate (7 mL/min). Coronal (b) and axial (d) slices from a T2w image of a mouse perfused with powder PFA and low flow rate (1 mL/min). Arrowheads indicate the hyperintense rim artifact.

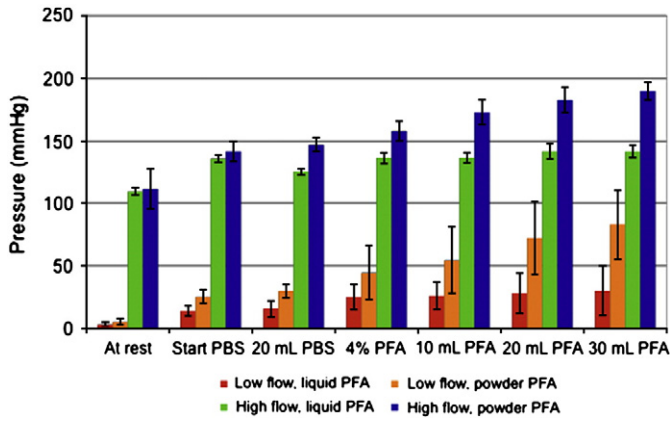


Fig. 2. Plot of pressure (mm Hg) at different time points during the transcatheter perfusion for the conditions summarized in Table 1. Error bars represent a 95% confidence interval.

isotropic voxels. In the first phase-encode dimension, consecutive k-space lines were assigned to alternating echoes to move discontinuity-related ghosting artifacts to the edges of the FOV (Thomas et al., 2004). This scheme necessitates oversampling in the phase-encode direction to avoid interference of the ghosts with the main image. This first phase-encode was oversampled by a factor of 2 (504 phase-encode points) giving a FOV of 28 mm that was subsequently cropped to 14 mm after reconstruction. Total imaging time was 11.7 hours.

T_2 relaxation maps were acquired for both a medial axial and sagittal slice using a multi-slice spin-echo sequence with eleven different TEs ranging from 0.008 to 0.1 s. The imaging parameters used were TR = 2000 ms, FOV = 28 × 14 mm, matrix size = 256 × 128, slice thickness = 0.5 mm and 2 averages.

Results

Hyperintense rim around the brain

A typical T2-weighted anatomical brain image is shown in Fig. 1a,c. Of the 30% of fixed brain samples received from collaborators with image artifacts, the majority (~500 samples from 13 different collaborators) displayed a hyperintense rim below the dura mater in T2-weighted MR images (Fig. 1b,d). The rim is typically less than 150 μm in width at the posterior aspect of the brain and up to 500 μm in width in the ventral-lateral part of the anterior aspect of the brain (arrowheads in Fig. 1b). Occasionally the rim is continuous around the entire brain but often there are breaks in the rim, particularly around the dorsal-posterior aspect (Fig. 1d). Upon removal of the skull, a thin blister of liquid was visible below the dura mater.

From a careful comparison of the various perfusion protocols used by several of our collaborators, two factors that were inconsistent during fixation were the perfusion flow rate and the form of the PFA solution. The cause of the hyperintense rim was investigated by systematically varying the perfusion flow rate and the form of the PFA solution (Table 1). The combination of powder PFA and high perfusion flow rate (7 mL/min) always reproduced the hyperintense rim around the brain in MR images. However, powder PFA and low perfusion flow rate (1 mL/min) only resulted in the hyperintense rim in 50% of the images. The use of liquid PFA, regardless of the flow rate (7 or 1 mL/min), never showed a hyperintense rim.

To examine why the artifact appears to be dependent on the form of the PFA solution, the perfusion flow rate was kept constant (7 or 1 mL/min) and the pressure (mm Hg) at entry to the left ventricle was measured using a pressure transducer. Fig. 2 shows the pressure at several time points throughout the entire

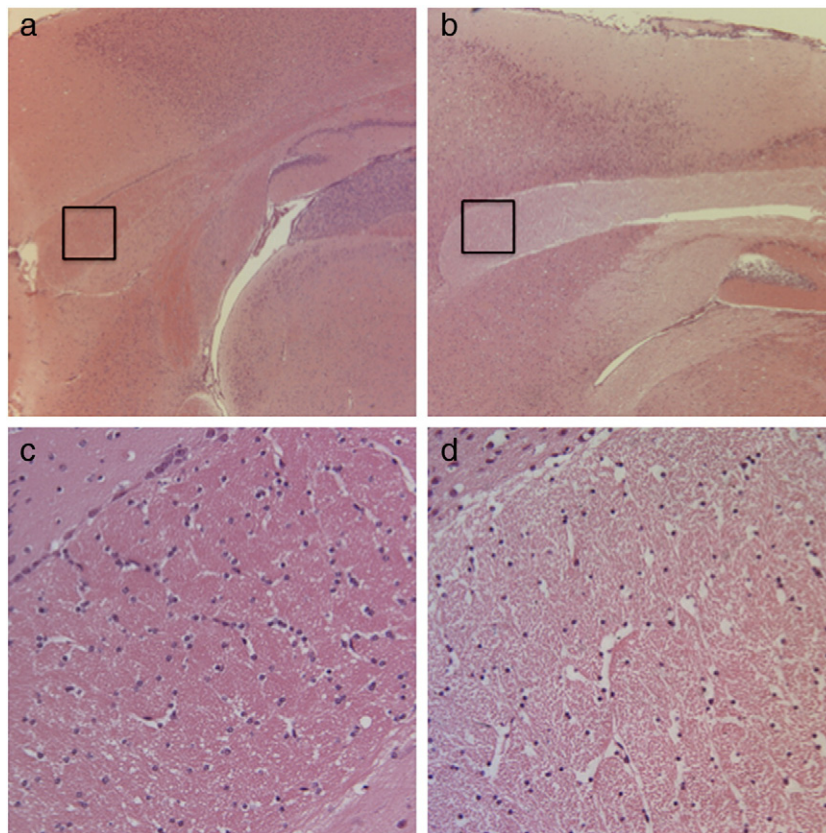


Fig. 3. H&E stained sagittal sections for tissue fixed with (a), (c) 4% PFA and (b), (d) 0.5% PFA. The top and bottom images were taken at 5× and 40× resolution respectively.

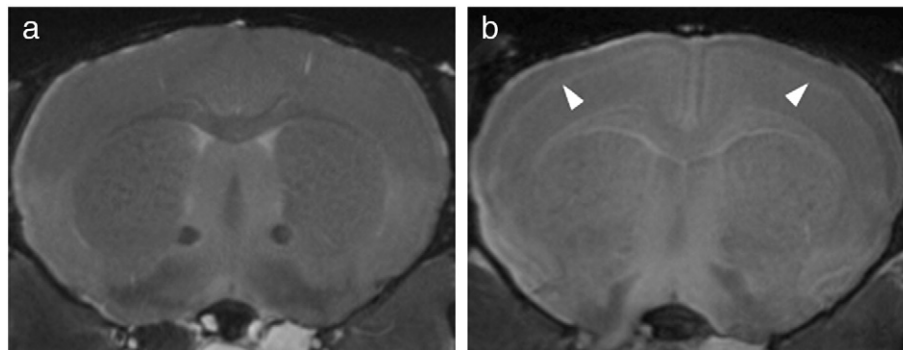


Fig. 4. (a) Coronal slice from a T2w MR image of a mouse perfusion fixed with 4% PFA. (b) Coronal slice from a T2w MR image of a mouse inadequately perfusion fixed with 0.5% PFA. Arrowheads indicate a hyperintense band in the cortical gray matter.

transcardiac perfusion. At a flow rate of 7 mL/min, the pressure is significantly higher than at 1 mL/min. When perfusing with powder PFA at both high and low flow rate, the pressure towards the end of the perfusion appears higher than with liquid PFA. This difference is even more pronounced in the high flow rate condition. In addition, the pressure even before the addition of PFA is higher in the powder PFA perfusion conditions, where powder rather than liquid PBS is used. The increase in pressure observed with both powder PFA and powder PBS suggests that some vascular blockage is occurring in the brain during perfusion.

Inverse gray–white matter contrast

The effect of the concentration of liquid PFA used for fixation was examined using conventional H&E staining and MR imaging. In comparison to the tissue in a well fixed brain (Fig. 3a), the tissue fixed with 0.5% PFA has areas of vacuolization and loss of cytoplasm (Fig. 3b). This is most pronounced in the white matter structures such as the corpus callosum (Fig. 3d). Here, the nuclei are smaller and many appear to have lost their chromatin pattern. This description is consistent with tissue and cell degradation, resulting from inadequate fixation.

It is well established that fixation with PFA significantly reduces the T_1 and T_2 relaxation rates of tissue, thereby altering MR contrast (Blamire et al., 1999; Kamman et al., 1985; Shepherd et al., 2009a; 2009b; Tovi and Ericsson, 1992). In T2-weighted MR images of fixed

brains, the white matter structures are hypointense relative to the gray matter structures (Figs. 1 and 4a). Fig. 4b shows the difference in gray–white matter contrast that is observed following inadequate fixation. This artifact was observed to some degree in approximately 5% of the fixed MR brain images acquired at our laboratory. Many of the white matter structures (i.e. corpus callosum, fimbria, fornix, medulla, arbor vita of cerebellum, internal capsule) now appear hyperintense and in some parts isointense to the gray matter structures (i.e. cortex, hippocampus, amygdala, thalamus, hypothalamus). This artifact results when the fixation time is too short or when the concentration of PFA is too low. There is also evidence of an artifact that appears as a hyperintense band in the cortical gray matter (arrowheads Fig. 4b). A similar hyperintense band has also been reported in human brain tissue at early time points during fixation (Blamire et al., 1999).

Starting with a well fixed brain with normal contrast (Fig. 5a), Fig. 5 shows the reversal of gray–white matter contrast as the concentration of PFA is decreased. Fig. 6 shows T_2 relaxation maps for the brains fixed with 4% and 0.5% PFA. The T_2 values for gray and white matter are summarized in Table 2. Considering the difference in field strength, the T_2 relaxation rates for the sample fixed with 4% PFA are consistent with the T_2 value reported by Shepherd et al. for gray matter in rat brain tissue fixed with 4% PFA (19 ± 2 ms at 17.6 T) (Shepherd et al., 2009b). If tissue is not adequately fixed, the T_2 value of white matter remains long (Tovi and Ericsson, 1992) and white matter structures appear hyperintense in T2-weighted images. The change in signal

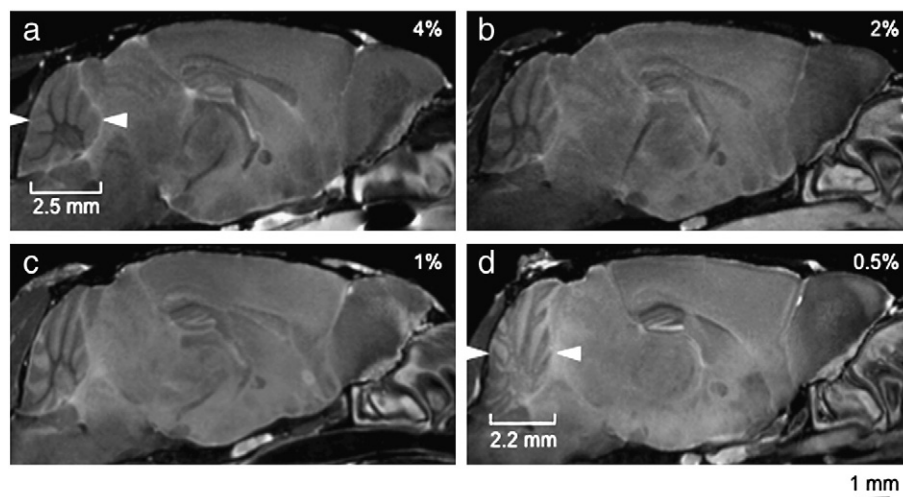


Fig. 5. Sagittal slices from T2w images of four brains perfusion fixed with decreasing concentration of PFA: (a) 4%, (b) 2%, (c) 1% and (d) 0.5%. Scale bar is 1 mm. Arrowheads indicate deformation of the cerebellum in the rostral–caudal aspect from 2.5 mm in the well fixed brain to 2.2 mm in the brain fixed with 0.5% PFA.

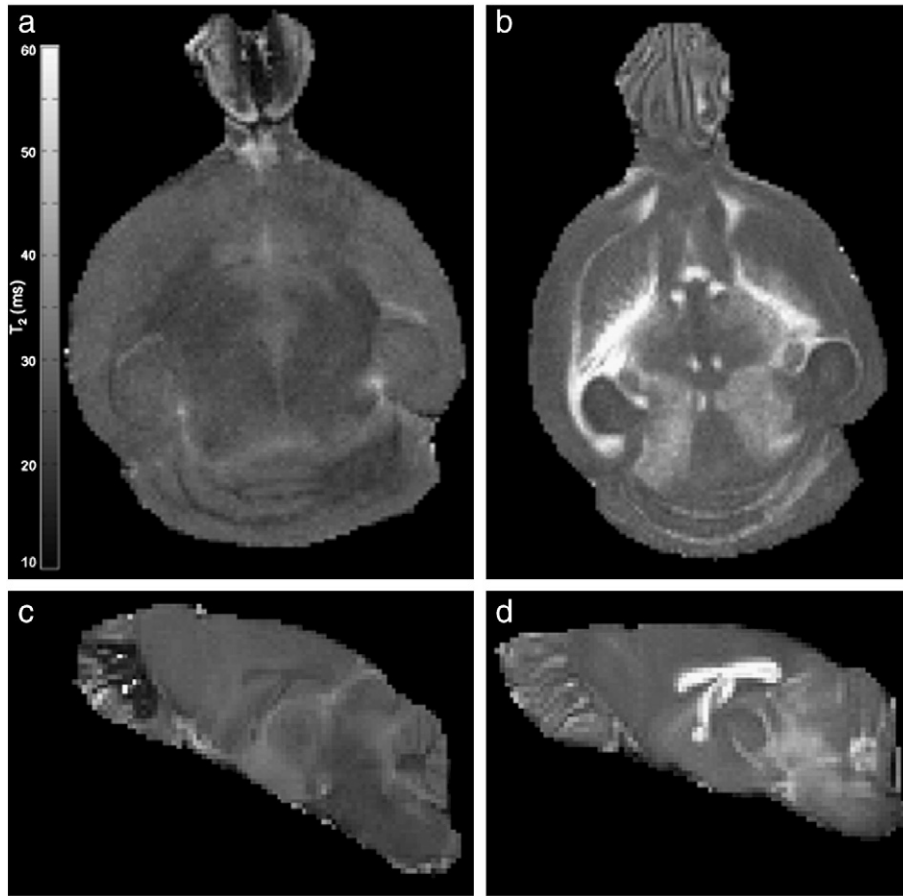


Fig. 6. Representative axial and sagittal T_2 relaxation maps for brains perfusion fixed with (a), (c) 4% PFA and (b), (d) 0.5% PFA.

intensity difference between gray and white matter with PFA concentration is summarized in Fig. 7. At 2% PFA the contrast appears reversed and is comparable to that of the well fixed brain. The contrast in the well fixed brain is consistent with published fixed MR images. As the concentration of PFA is decreased, there is an overall increase in the SNR. In the sagittal slices in Fig. 5, the mean SNR in the brain fixed with 0.5% PFA was 40% higher than the well fixed brain.

Although the longer white matter T_2 values result in higher SNR for poorly fixed samples, the images cannot be used for quantitative data analysis. A significant consequence of inadequate fixation is deformation of the brain tissue. Fig. 5c and d clearly show that the cerebellum has been distorted, extending higher into the dorsal-posterior aspect of the meninges. This deformation is always found in images with inverse gray–white matter contrast. Thus, the presence of inverse contrast can act as a signature of inadequate tissue fixation and the associated deformation of anatomical structures such as the cerebellum.

Discussion

The cerebral vasculature has a well-defined structure that is highly arborized and is patterned such that all cells are, on

average, within 100 μm of a vessel (Beard and Bassingthwaite, 2001). During transcatheter perfusion, the perfusates travel from the arteries to the capillary beds and the pressure decreases gradually along this branched network. The pressure measurements shown in Fig. 2 were not imposed directly at the capillary beds but indicate increased pressure throughout the cerebral vasculature. Particles of undissolved PFA or PBS in the solution could cause blockages in some of the capillaries. This blockage would

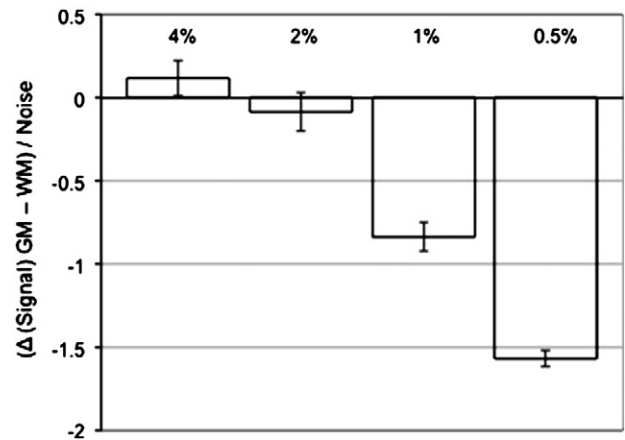


Fig. 7. Plot of signal intensity difference between gray matter (GM) and white matter (WM) divided by the noise at different concentrations of PFA. Error bars represent a 95% confidence interval. The mean SNR values for gray and white matter were measured for the cortex and corpus callosum in the sagittal slices in Fig. 5.

Table 2

T_2 relaxation rates for the gray and white matter at different concentrations of PFA for fixation. The mean T_2 values were determined and averaged for the corpus callosum, internal capsule and the cortex from the axial and sagittal slices shown in Fig. 6.

PFA concentration	T_2 gray matter (ms)	T_2 white matter (ms)
0.5%	27 ± 1	60 ± 5
4%	27 ± 1	24 ± 1

increase the pressure at the capillaries to the point of leakage of the perfusate and even rupture, producing extra vascular liquid that could migrate to just below the dura mater.

The acquisition of high resolution 3D MR images of fixed brain samples allows for automated and quantitative morphological analysis. Through the use of digital segmented atlases and voxel-based morphometry, volume changes of identifiable anatomical structures and localized differences in size, shape and position throughout the brain can be determined. Results of this kind are valuable, for example, in phenotypic screening and the study of mammalian development (Henkelman, 2010; Nieman et al., 2011). To use these tools, the MR images must first be accurately registered. This is done using automated image registration methods that are based on matching voxel intensities. Registration of the MR images that display the hyperintense rim fails because the rim aligns better with the cortex than the dark meninges and skull. This prevents accurate identification of the cortical surface by the registration algorithm. Segmenting of the bright rim in the images by thresholding might appear to be a plausible solution but, in a cohort of C57BL/6J adult mice perfused with powder PFA and high perfusion flow rate, an inverse correlation was found between the volume of the hyperintense rim and the volume of the total brain (data not shown). The volume of the total brain was found to decrease by up to 22% ($p = 1.49 \times 10^{-6}$) when the rim was severe. This suggests that the blister of liquid results in increased pressure that shrinks the brain and/or that the liquid is invading the parenchyma. This observation invalidates accurate morphological assessment of changes in structural volume and limits the ability to attribute these changes to genetic differences.

In addition, reliable registration is not possible in a group of images with inverse gray–white matter contrast. Most importantly, the deformation of the cerebellum represents a confounder to the registration method and yields unreliable morphometry. The inverse contrast is also problematic for registration. For example, when matching the corpus callosum (hyperintense) in images with inverse contrast, a higher correlation is found to the cortex than to the corpus callosum (hypointense) in typical fixed MR images and therefore the corpus callosum will incorrectly register to the cortex.

Conclusions

Image SNR and contrast-to-noise ratio (CNR) depend upon the quality of the fixation and therefore it is important to standardize perfusion protocols. This paper is not meant to be an exhaustive study of MR artifacts in fixed mouse brain samples. Two artifacts most commonly found in images acquired at our laboratory were presented and found to result from the use of powder perfusates, high perfusion flow rate and inadequate fixation. It has been noted by one of the referees that the use of “stale” heparin during perfusion also results in similar MR artifacts. These fixation artifacts are unacceptable for quantitative data analysis and in most cases where they were observed, the collaborators had to prepare new samples. For accurate interpretation and to avoid fixation artifacts and minimize the number of animals used, the concentration (2–4%) and form of the PFA solution (liquid PFA) are critical. A low perfusion flow rate plays an additional role in minimizing fixation artifacts.

Acknowledgments

The Mouse Imaging Centre acknowledges funding from the Canada Foundation for Innovation and the Ontario Innovation Trust for providing facilities along with The Hospital for Sick Children. Operating funds from the Canadian Institutes of Health Research, Genome

Canada, the National Cancer Institute of Canada–Terry Fox Program Projects, the National Institutes of Health, Ontario Institute for Cancer Research, Ontario Research Fund, and the Ontario Research and Development Challenge Fund are gratefully acknowledged. LSC holds a CIHR postdoctoral fellowship and RMH holds a Canada Research Chair in Imaging.

References

- Badea, A., Ali-Sharief, A.A., Johnson, G.A., 2007. Morphometric analysis of the C57BL/6J mouse brain. *NeuroImage* 37, 683–693.
- Beard, D.A., Bassingthwaite, J.B., 2001. Modeling advection and diffusion of oxygen in complex vascular networks. *Ann. Biomed. Eng.* 29, 298–310.
- Blamire, A.M., Rowe, J.G., Styles, P., McDonald, B., 1999. Optimising imaging parameters for post mortem MR imaging of the human brain. *Acta Radiol.* 40, 593–597.
- Chuang, N., Mori, S., Yamamoto, A., Jiang, H., Ye, X., Xu, X., Richards, L.J., Nathans, J., Miller, M.I., Toga, A.W., Sidman, R.L., Zhang, J., 2011. An MRI-based atlas and database of the developing mouse brain. *NeuroImage* 54, 80–89.
- Dazai, J., Spring, S., Cahill, L.S., Henkelman, R.M., 2011. Multiple-mouse neuroanatomical magnetic resonance imaging. *J. Vis. Exp.* 48, e2497.
- Dorr, A.E., Lerch, J.P., Spring, S., Kabani, N., Henkelman, R.M., 2008. High resolution three-dimensional brain atlas using an average magnetic resonance image of 40 adult C57BL/6J mice. *NeuroImage* 42, 60–69.
- Ellegood, J., Pacey, L.K., Hampson, D.R., Lerch, J.P., Henkelman, R.M., 2010. Anatomical phenotyping in a mouse model of fragile X syndrome with magnetic resonance imaging. *NeuroImage* 53, 1023–1029.
- Ellegood, J., Lerch, J.P., Henkelman, R.M., 2011. Brain abnormalities in a *Neuroigin3* R451C knockin mouse model associated with autism. *Autism Res.* 4, 368–376.
- Henkelman, R.M., 2010. Systems biology through mouse imaging centers: experience and new directions. *Annu. Rev. Biomed. Eng.* 12, 143–166.
- Ho, S.K.Y., Kovacevic, N., Henkelman, R.M., Boyd, A., Pawson, T., Henderson, J.T., 2009. EphB2 and EphA4 receptors regulate formation of the principal inter-hemispheric tracts of the mammalian forebrain. *Neuroscience* 160, 784–795.
- Kamman, R.L., Go, K.G., Stomp, G.P., Hulstaert, C.E., Berendsen, H.J., 1985. Changes of relaxation times T1 and T2 in rat tissues after biopsy and fixation. *Magn. Reson. Imaging* 3, 245–250.
- Kim, J.J., Gill, P.S., Rotin, L., van Eede, M., Henkelman, R.M., Hui, C.C., Rosenblum, N.D., 2011. Suppressor of fused controls mid-hindbrain patterning and cerebellar morphogenesis via *GLI3* repressor. *J. Neurosci.* 31, 1825–1836.
- Lau, J.C., Lerch, J.P., Sled, J.G., Henkelman, R.M., Evans, A.C., Bedell, B.J., 2008. Longitudinal neuroanatomical changes determined by deformation-based morphometry in a mouse model of Alzheimer's disease. *NeuroImage* 42, 19–27.
- Lerch, J.P., Carroll, J.B., Dorr, A., Spring, S., Evans, A.C., Hayden, M.R., Sled, J.G., Henkelman, R.M., 2008a. Cortical thickness measured from MRI in the YAC128 mouse model of Huntington's disease. *NeuroImage* 41, 243–251.
- Lerch, J.P., Carroll, J.B., Spring, S., Bertram, L.N., Schwab, C., Hayden, M.R., Henkelman, R.M., 2008b. Automated deformation analysis in the YAC128 Huntington disease mouse model. *NeuroImage* 39, 32–39.
- Lerch, J.P., Yiu, A.P., Martinez-Canabal, A., Pekar, T., Bohbot, V.D., Frankland, P.W., Henkelman, R.M., Josselyn, S.A., Sled, J.G., 2011. Maze training in mice induces MRI-detectable brain shape changes specific to the type of learning. *NeuroImage* 54, 2086–2095.
- Ma, Y., Hof, P.R., Grant, S.C., Blackband, S.J., Bennett, R., Slates, L., McGuigan, M.D., Benveniste, H., 2005. A three-dimensional digital atlas database of the adult C57BL/6J mouse brain by magnetic resonance microscopy. *Neuroscience* 135, 1203–1215.
- Mercer, R.E., Kwolok, E.M., Bischof, J.M., van Eede, M., Henkelman, R.M., Wevrick, R., 2009. Regionally reduced brain volume, altered serotonin neurochemistry, and abnormal behavior in mice null for the circadian rhythm output gene *Magel2*. *Am. J. Med. Genet. B Neuropsychiatr. Genet.* 150B, 1085–1099.
- Nieman, B.J., Wong, M.D., Henkelman, R.M., 2011. Genes into geometry: imaging for mouse development in 3D. *Curr. Opin. Genet. Dev.* 21, 638–646.
- Sawiak, S.J., Wood, N.I., Williams, G.B., Morton, A.J., Carpenter, T.A., 2009. Use of magnetic resonance imaging for anatomical phenotyping of the R6/2 mouse model of Huntington's disease. *Neurobiol. Dis.* 33, 12–19.
- Shepherd, T.M., Flint, J.J., Thelwall, P.E., Stanisz, G.J., Mareci, T.H., Yachnis, A.T., Blackband, S.J., 2009a. Postmortem interval alters the water relaxation and diffusion properties of rat nervous tissue—implications for MRI studies of human autopsy samples. *NeuroImage* 44, 820–826.
- Shepherd, T.M., Thelwall, P.E., Stanisz, G.J., Blackband, S.J., 2009b. Aldehyde fixative solutions alter the water relaxation and diffusion properties of nervous tissue. *Magn. Reson. Med.* 62, 26–34.
- Song, S.K., Yoshino, J., Le, T.Q., Lin, S.J., Sun, S.W., Cross, A.H., Armstrong, R.C., 2005. Demyelination increases radial diffusivity in corpus callosum of mouse brain. *NeuroImage* 26, 132–140.
- Spring, S., Lerch, J.P., Henkelman, R.M., 2007. Sexual dimorphism revealed in the structure of the mouse brain using three-dimensional magnetic resonance imaging. *NeuroImage* 35, 1424–1433.
- Thomas, D.L., De Vita, E., Roberts, S., Turner, R., Yousry, T.A., Ordidge, R.J., 2004. High-resolution fast spin echo imaging of the human brain at 4.7 T: implementation and sequence characteristics. *Magn. Reson. Med.* 51, 1254–1264.

- Tovi, M., Ericsson, A., 1992. Measurements of T1 and T2 over time in formalin-fixed human whole-brain specimens. *Acta Radiol.* 33, 400–404.
- Tyszka, J.M., Readhead, C., Bearer, E.L., Pautler, R.G., Jacobs, R.E., 2006. Statistical diffusion tensor histology reveals regional dysmyelination effects in the shiverer mouse mutant. *Neuroimage* 29, 1058–1065.
- Wetzel, M.K., Naska, S., Laliberte, C.L., Rymar, V.V., Fujitani, M., Biernaskie, J.A., Cole, C.J., Lerch, J.P., Spring, S., Wang, S.H., Frankland, P.W., Henkelman, R.M., Josselyn, S.A., Sadikot, A.F., Miller, F.D., Kaplan, D.R., 2008. p73 regulates neurodegeneration and phospho-tau accumulation during aging and Alzheimer's disease. *Neuron* 59, 708–721.
- Yu, X., Nieman, B.J., Sudarov, A., Szulc, K.U., Abdollahian, D.J., Bhatia, N., Lalwani, A.K., Joyner, A.L., Turnbull, D.H., 2011. Morphological and functional midbrain phenotypes in Fibroblast Growth Factor 17 mutant mice detected by Mn-enhanced MRI. *Neuroimage* 56, 1251–1258.
- Zhang, J., Richards, L.J., Yarowsky, P., Huang, H., van Zijl, P.C.M., Mori, S., 2003. Three-dimensional anatomical characterization of the developing mouse brain by diffusion tensor microimaging. *Neuroimage* 20, 1639–1648.
- Zhang, X., Bearer, E.L., Boulat, B., Hall, F.S., Uhl, G.R., Jacobs, R.E., 2010. Altered neurocircuitry in the dopamine transporter knockout mouse brain. *PLoS One* 5, e11506.